



CHORUS

This is the accepted manuscript made available via CHORUS. The article has been published as:

Temperature-dependent thermal conductivity and suppressed Lorenz number in ultrathin gold nanowires

S. D. Sawtelle and M. A. Reed

Phys. Rev. B **99**, 054304 — Published 12 February 2019

DOI: [10.1103/PhysRevB.99.054304](https://doi.org/10.1103/PhysRevB.99.054304)

Temperature Dependent Thermal Conductivity and Suppressed Lorenz Number in Ultrathin Gold Nanowires

S. D. Sawtelle* and M. A. Reed

Departments of Applied Physics and Electrical Engineering, Yale University, New Haven, CT 06520 USA

(Dated: December 17, 2018)

The values of material parameters required for quantitative electrothermal modeling of nanoscale structures typically differ strongly from those of the bulk material. In this work we apply a simple experimental technique that allows us to estimate values for thermal conductivity of both a metal nanowire and its insulating substrate by measuring the increase in resistance due to small amounts of DC self-heating. We measure gold nanowires with widths between 24 and 55 nm using this technique, and extract relevant material parameters as a function of temperature. Electrical resistivities of our nanowires are width-dependent and much higher than bulk gold values, and enhanced temperature-dependence of the resistivity indicates a depressed Debye temperature due to significant phonon softening. The fit thermal conductivity versus temperature of our 21 nm SiO₂ on Si substrate is highly consistent with literature values for oxide thin films. We find the thermal conductivity of the nanowires increases rapidly with temperature and width and is well below the value for bulk gold, which can be qualitatively explained by the dominance of structural scattering. The Lorenz number is relatively constant over temperature, as in the Wiedemann-Franz theory, but it is significantly lower than reported values for bulk gold and exhibits some width dependence.

I. INTRODUCTION

The continual scaling down of device structures and the rise of nanostructured materials has created a need to characterize and understand electrothermal properties at the nanoscale. It has been well established that electric and thermal conduction in metal nanostructures is generally suppressed relative to bulk metals due to the increasing influence of surface and grain boundary scattering¹⁻³. Electrical conductivity is straightforward to measure and has been thoroughly characterized for a wide variety of metal nanowires⁴⁻⁷, while the thermal conductivity of these systems has proven much more challenging to assess.

Measurements of thermal conductivity of individual metal nanowires have previously taken pains to eliminate all parasitic heat sinking, and consequently restricted measurements to wire geometries and microstructures which can be fabricated as fully suspended⁸⁻¹². Here we demonstrate that by incorporating substrate coupling into the thermal model and varying nanowire length as an experimental parameter, it is possible to measure top-down substrate-coupled wires and fit values for both the substrate and nanowire thermal conductivity.

For studies that measure both electrical and thermal conductivity we may compute the Lorenz Ratio $L := \frac{\kappa}{\sigma T}$, with κ the thermal conductivity, σ the electrical conductivity, and T the temperature. The Wiedemann-Franz (WF) law asserts that L should be constant across all metals and temperatures, and equal to $L_0 = 2.44\text{e-}8 \text{ W}\cdot\Omega / \text{K}^2$ within the Sommerfeld theory of metals¹³. The basic observation underlying WF is that electrons are the primary carriers of both charge and thermal energy, and that scattering of those carriers identically impedes their ability to transport both quantities. This simple relationship holds surprisingly well, but L for many bulk metals exhibits temperature-dependent deviations from

L_0 due to phonon-mediated thermal current and inelastic electron-phonon scattering¹⁴, both of which are neglected in the WF derivation.

A more careful statement of WF is that the ratio of the *electronic* thermal conductivity to the electrical conductivity is constant: $L_e := \frac{\kappa_e}{\sigma T} = L_0$. Consequently if phonon contributions to the thermal current, κ_{ph} , cannot be neglected then the experimentally measured L ratio can be higher than the theoretical L_0 value¹⁵. On the other hand, this expression for L_e still neglects the effect of electron-phonon inelastic scattering processes with low energy phonons - a process which tends to lower the L ratio. When electrons exchange energy with small- q phonons they are scattered through only a small angle and the thermal current is relaxed more effectively than the drift momentum of the electrons is randomized. Thus κ_e is suppressed disproportionately to σ when small-angle scattering is dominant^{14,16}, which typically occurs below the Debye temperature wherein only small- q modes are occupied. As the temperature rises and high- q phonon modes with much larger density of states become occupied, fully-randomizing large-angle scattering dominates and L_e is expected to approach L_0 .

Systems with significant electron-electron scattering can also have reduced L values,^{17,18} as normal scattering processes can randomize thermal energy between hot and cold electrons while the total net momentum of the electron gas remains unchanged. However electron-electron interactions are typically considered negligible in metallic systems in the temperature range of interest¹⁹. Recently an order of magnitude suppression of L_e was observed in metallic vanadium oxide beyond its metal-insulator transition²⁰ and explained by the absence of quasiparticles in a highly correlated electron fluid.

Both the κ_{ph} and the small-angle scattering effects can help explain deviations of L_{bulk} values from the theoretical L_0 , and may also help explain deviations of L

in nanoscale metal structures from their corresponding L_{bulk} values. In the temperature range between 95 and 300 K a suppressed value of L relative to L_{bulk} has been reported for individual Pt⁹ and Ag¹¹ nanowires, while other works have instead found increased L for nanowires and thin films^{8,10,21,22}. Recently it has been proposed that non-negligible thermal contact resistance in a two-terminal measurement configuration may artificially inflate measured L values¹². Our results suggest that for highly granular, ultrathin gold nanowires on a substrate the Lorenz ratio is roughly constant over the range from 95 to 260 K although its value is significantly depressed compared to bulk, and appears to exhibit some wire width dependence.

Semiconducting nanowires also exhibit suppressed thermal and electrical conductivity relative to the bulk material, however in this case the primary heat carriers (phonons) and charge carriers (electrons) are different; thus the WF relation does not apply and the two conductivities are not as strongly coupled as in metals. Consequently semiconductor wires are attractive for thermoelectric applications like clean energy conversion²³, where the figure of merit (ZT) can be improved by selectively decreasing κ relative to σ . In contrast to metal nanowires, the mechanisms for suppression of κ in semiconductor nanowires include enhanced phonon surface and defect scattering^{24,25} and modified phonon dispersion due to confinement effects²⁶. Measurements of κ in semiconductor nanowires employ many of the same methods as for metal nanowires, including the DC self-heating approach which is expanded upon in this work²⁷.

II. METHODS

A. Device Design and Fabrication

Using an electron-beam lithography process, we fabricate top-down, ultrathin (22 nm) gold nanowires with no adhesion layer atop a very thin (22 nm) high quality thermal SiO₂ plus thick Si handle. Wire widths range from approximately 20 to 60 nm and lengths range from 600 to 1500 nm, as estimated by high-resolution SEM. As illustrated by the schematic and SEM characterization in Fig. 1, in the active region of each device a thin gold nanowire or nanoconstriction is bookended by large triangular contact areas, which are overlapped by a 100 nm thick Ti/Au contact layer that rapidly tapers out to the wide on-chip vias. Because we omit an adhesion layer for the gold nanowire structure, the deposition parameters of the thin metal and the temperature of all subsequent processing must be very carefully controlled.

B. Thermal Model for Self-Heating

We utilize an analytical model formulated by Hunley et al.²⁸ for the temperature increase under DC Joule

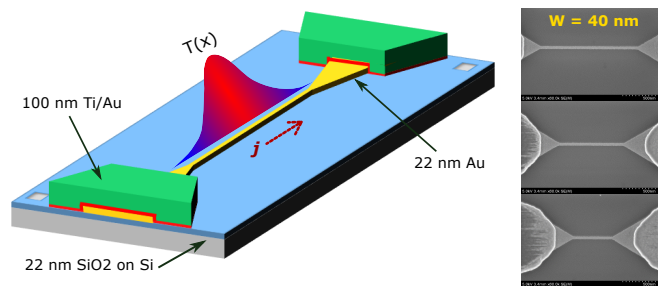


FIG. 1. Schematic of the wire geometry with DC self-heating conceptualized (left) and SEM of the active region of devices for a series of nanowire lengths and fixed width (right).

self-heating in metal nanowires, which incorporates both thermal coupling to the wire's underlying substrate²⁹ and heat spreading into a finite contact region. Due to the thermal conductivity of the inert gas being much lower than that of the nanowire metal and even the oxide substrate, as well as the relatively short lengths of the wires employed in our work, convective heat losses to the gaseous environment are neglected^{9,30,31}.

The physical model comprises a narrow metal wire connected to much larger pad regions, defined on a thermally insulating layer atop a thermally conductive back gate at the bath temperature (the thick Si handle of our chips). We define the following quantities: W , τ_n and ℓ are the wire width, thickness and length (between the two contact pads), κ_n and κ_{ox} are the thermal conductivities of the nanowire and oxide, and d is the thickness of the oxide. The nanowire sustains a uniform current density of J and resistivity of ρ . The \hat{x} axis points along the length of the nanowire, which is centered around $x=0$.

Hunley et al.²⁸ have derived an approximate heat equation governing the excess temperature, T_e , in the wire:

$$\nabla^2 T_e(x) - m_1^2 T_e(x) = -\frac{Q}{\kappa_n}, \quad (1)$$

$$m_1^2 = \frac{\kappa_{ox}\pi}{W\tau_n\kappa_n \ln\left(\frac{d}{W}(2+\pi) + e^{-\frac{2d}{W}}\right)},$$

$$Q = J^2\rho.$$

For our application of very small self-heating, we assume the resistivity of the nanowire in an environmental temperature T_0 can be well approximated as a constant $\rho(T_0)$ everywhere, despite the non-uniform temperature profile along the length of the wire. We also assume that under such small heating there is negligible heat spreading into the contacts and they act as perfect heat sinks clamped at T_0 , so that $T_e(\ell/2) = T_e(-\ell/2) = 0$. With these

boundary conditions the solution to Eq. (1) becomes

$$T_e = A \cosh\left(\sqrt{\frac{\lambda}{\kappa_n}} x\right) + \frac{Q}{\lambda},$$

$$\lambda = \frac{\pi \kappa_{ox}}{W \tau_n \ln\left(\frac{d}{W}(2 + \pi) + \exp(-2d/W)\right)},$$

$$A = -\frac{Q}{\lambda} \cosh^{-1}\left(\sqrt{\frac{\lambda}{\kappa_n}} \frac{\ell}{2}\right).$$

The composite parameter λ quantifies how effectively heat can be sunk to the substrate: it is large if κ_{ox} is large, or if the cross-sectional area of the wire is small so that the perimeter to cross-sectional area ratio is large, or if the insulating substrate is thin relative to the width of the wire so that the wire is well coupled to the conductive back gate.

The average increase in temperature over the length of the wire due to this heating is

$$\Delta T = \frac{1}{\ell} \int_{-\ell/2}^{\ell/2} T_e dx = \frac{Q}{\lambda} \left[1 - \frac{\tanh(\gamma)}{\gamma}\right].$$

Here $\gamma = \sqrt{\frac{\lambda}{\kappa_n}} \frac{\ell}{2}$ is a dimensionless tuning parameter that quantifies the relative efficacies of the two heat sinking mechanisms (substrate versus along-wire), and dictates how the temperature rise will depend on the material parameters embodied in λ and κ_n . When substrate heat sinking is negligible compared to heat transfer along the nanowire (λ is very small or κ_n is very large or ℓ is very short) then γ is small. In that case $\frac{\tanh(\gamma)}{\gamma} \approx 1 - \frac{1}{3}\gamma^2$ and the expression reduces to that used in Refs. 8 and 9, which depends on κ_n but not λ . If instead substrate heat sinking dominates the heat diffusion path along the nanowire, then γ grows large and $\frac{\tanh(\gamma)}{\gamma} \approx 1/\gamma \ll 1$, so that the average temperature rise depends on λ but not κ_n . Specifically, the two limiting behaviors are

$$\Delta T \approx \frac{Q\ell^2}{12\kappa_n} \text{ for } \gamma \ll 1 \text{ (wire heat sinking),}$$

$$\Delta T \approx \frac{Q}{\lambda} \text{ for } \gamma \gg 1 \text{ (substrate heat sinking).}$$

This temperature rise due to self-heating induces a corresponding change in the resistance of the wire due to the temperature-dependence of electrical resistivity. The change in resistance per small unit of I^2 can be found as follows

$$\Delta R = \frac{dR}{dT} \Delta T = \frac{\ell}{A} \frac{d\rho}{dT} \cdot \frac{Q}{\lambda} \cdot \left[1 - \frac{\tanh(\gamma)}{\gamma}\right]$$

$$\Rightarrow \frac{dR}{d(I^2)} \approx \frac{\Delta R}{\Delta(I^2)} = \frac{d\rho}{dT} \frac{\rho \ell}{\lambda A^3} \cdot \left[1 - \frac{\tanh(\gamma)}{\gamma}\right] \quad (2)$$

We see that the resistance should increase linearly with I^2 , where the self-heating slope $m = \frac{dR}{d(I^2)}$ depends on

the material and geometrical properties of the wire. Figure 2 demonstrates this concept with room temperature measurements of R vs. I^2 for three different prototypical structures. The large on-chip via structures have effectively zero self-heating, the bowtie structures which are extremely well coupled to the contact pads have only moderate self-heating slopes, while the longer wires have the most significant self-heating slopes.

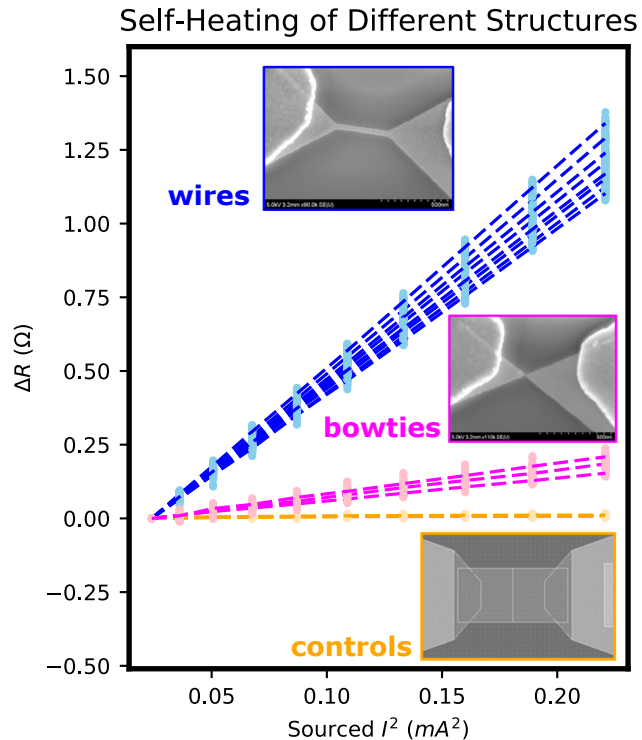


FIG. 2. Comparison of the resistance increase due to self-heating for three different geometries at room temperature. Several devices are measured for each geometry, and for each device multiple repeated traces are plotted (points) together with the linear fit (dashed lines). All devices conform extremely well to the thermal model of resistance increasing linearly with I^2 .

The relationship embodied in Eq. (2) supports a simple experimental technique for extracting temperature-dependent nanowire material parameters. Over a range of environmental temperatures we measure R vs. I^2 for a set of nanowires of varying length but fixed width. The zero-bias resistances allows us to compute $\rho(T)$ and thus also estimate the temperature dependence $d\rho/dT$. The measured self-heating slope as a function of length at each temperature can then be used to fit values for κ_{ox} and κ_n at that temperature.

Because $\kappa_{ox}(T)$ does not depend on wire width, it only needs to be estimated once by the above method. We can then supply $\kappa_{ox}(T)$ as a known parameter for all other widths of wires and simply compute $\kappa_n(T)$ from the measured self-heating slope, obviating the need to

measure a set of different lengths for each width.

We note in closing this section that the two extreme cases of very small and large γ predict a very different wire length dependence for the self-heating slope $m = \frac{dR}{d(I^2)}$ at a given fixed width: proportional to ℓ^3 in the case of small γ , and only proportional to ℓ in the other extreme. No clear width-dependence under fixed length can be derived because ρ , $d\rho/dT$, and κ_n will all have nontrivial width dependence.

C. Measurement Setup

We use a Keithley 2400 SMU to source a current while monitoring the voltage with source readback enabled. To minimize error we program a 50 ms source-measure delay, integrate for several power line cycles for each reading, and repeat our voltage sweep 8 times in order to obtain a more robust estimate of $\frac{dR}{d(I^2)}$. To minimize the offset error of the reading we implement a protocol of first setting the sourced current to zero through the device and measuring the voltage ten times; the average zero bias voltage is then subtracted from all values in the subsequent sweep. Testing our protocol on macroscopic resistors which experience effectively zero self-heating confirms that the systematic error in ΔR is less than 50 m Ω over the relevant current range.

Our variable temperature measurements employ a Janis Research SuperVariTemp (SVT) cryostat with a high-throughput sample probe, incorporating a resistive wound heater and thermometry on the sample mount. Prior to the experiments a temperature calibration experiment was performed in order to obtain a mapping from the probe thermometry readings to the true chip surface temperature during active heating with the wound heater. Figure 3a shows the experimentally measured self-heating curves obtained at different environmental temperatures for an example wire device; the changing slope stems from changes in ρ , κ_{ox} and κ_n with temperature. Figure 3b shows the corresponding self-heating slope and zero-bias device resistance extracted at each temperature.

III. EXPERIMENTAL

A. Estimates of Resistivity

Our devices are fabricated with large, temperature-dependent on-chip series resistance (long, narrow vias), and they do not have a four-terminal configuration that would allow us to interrogate only the nanowire resistance. Therefore to estimate nanowire $\rho(T)$ we first measured a test structure containing only the on-chip vias and cryostat leads to obtain an estimate of $R(T)$ for the series resistance. Additionally, for one width ($W = 40$ nm) we were able to measure total resistance for a set

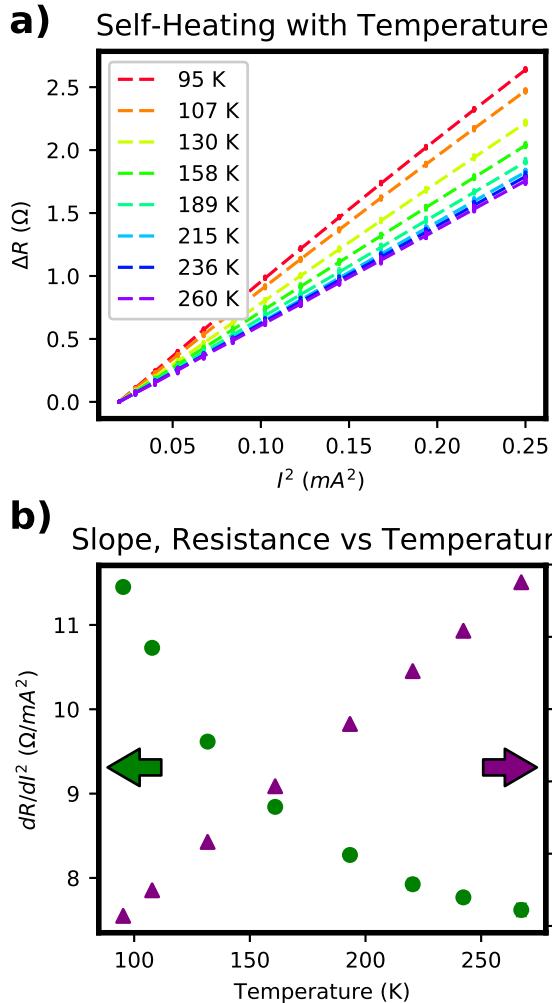


FIG. 3. Measurements of self-heating curves at different environmental temperatures (a) and the corresponding extracted zero-bias resistance and self-heating slope (b) for an example $W=40$ nm device. In (b), error bars giving standard error of the mean from 8 consecutive traces are smaller than the plotted data points for both quantities.

of wires with varying length, and then fit a straight line to R vs. L . These fitted intercepts at different temperatures provide an alternative estimate of $R(T)$ for the series resistance, which agrees within 4% with the direct measurement of the test structure. For all analyses we used an average of these two measurements as our full estimate of $R(T)$ for the series resistance, and we subtract this from the total measured resistance to isolate the nanowire contribution.

The $\rho(T)$ curves obtained with this procedure were highly linear for all the wire widths. The extrapolated room temperature resistivities, shown in Fig. 4a, are much higher than bulk values and have a strong width dependence, especially for the smallest 24 nm width. Under Matthiessen's rule the total resistivity is the sum of contributions from all structural scattering (ρ_0) on grain

boundaries, interfaces and impurities, and the electron-phonon scattering. The electron-phonon component is commonly modeled by the Bloch-Gruneisen expression from semi-classical Boltzmann transport theory for metals so that

$$\rho(T) = \rho_0 + K_{el-ph} \left(\frac{T}{\Theta}\right)^5 \int_0^{\Theta/T} \frac{x^5}{(e^x - 1)(1 - e^{-x})} dx. \quad (3)$$

Here θ_D is the Debye temperature and K_{el-ph} is the electron-phonon coupling constant. This curve takes the form of a plateau at low- T , which reveals the limiting ρ_0 value, transitioning rapidly into a linear temperature-dependence.

We do not have measurements down to sufficiently low T to reveal the limiting structurally-induced resistivity. However we can roughly estimate these values by extrapolating our linear resistivity curves down to a temperature at which the ρ_0 plateau is typically achieved in similar systems. We take this value as $T = 25$ K^{7,32} and estimate that the ρ_0 component accounts for 75% and 83% of the total resistivity at $T = 250$ K for our largest (53 nm) and smallest (24 nm) wires, respectively. Thus we confirm that structural scattering dominates in our wires even near room temperature.

The values for $d\rho/dT$, plotted in Fig. 4b, do not show a strong width dependence. This is consistent with the temperature-dependent component of the resistivity deriving from phonon occupancy rather than structural scattering. As also observed by previous works on nanowires^{8,33} and nanofilms⁷, the values of $d\rho/dT$ are all significantly higher than bulk gold. This is thought to reflect a softening of the phonon modes due to an increased fraction of dangling bonds on external and internal (grain boundary) surfaces, which lowers the Debye temperature and enhances the temperature-dependence of the phonon occupancy and resultant scattering^{32,34,35}.

Under the Bloch-Gruneisen model the slope of resistivity with temperature in the linear regime, $d\rho/dT$, can be used to solve for the Debye temperature. Previous work has shown that the electron-phonon coupling constant, K_{el-ph} , is effectively constant for monocrystalline metal nanowires from 15 to 200 nm wide⁷ and for polycrystalline gold films from 12 to 46 nm thick³⁵. We therefore use a literature value of $K_{el-ph} = 6.23e-8$ $\Omega \cdot m$ for a 25 nm thick gold nanofilm³⁵ and solve numerically to obtain θ_D for three nanowire widths. The values, listed in Table I, are all vastly lower than the bulk Debye temperature, with the deviation increasing as the wire width shrinks. Note that solving at values of $T = 95$ K versus 250 K results in only a 1 degree variation θ_D , and estimates in the table are computed at $T = 200$ K.

B. Estimate of Oxide Thermal Conductivity

We measured the self-heating slope at variable temperatures in the cryostat and at room temperature for a

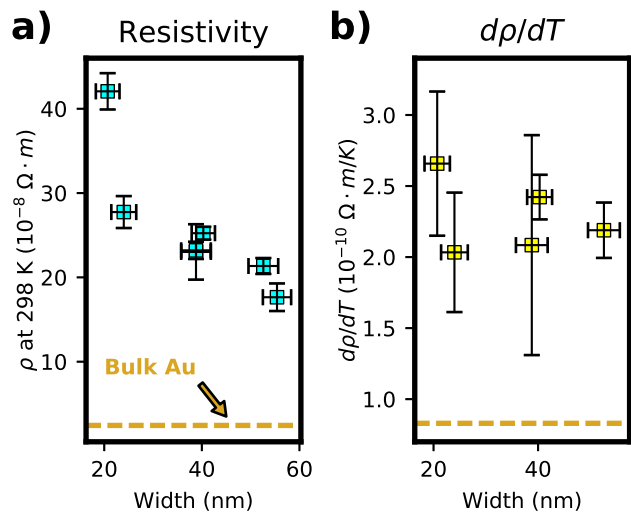


FIG. 4. Extrapolated room-temperature resistivities (a) and slope of resistivity with temperature (b) for a selection of wire widths. Horizontal error bars denote standard deviation of the SEM width measurements, while vertical error bars denote standard error of the mean.

TABLE I. The width (W), extrapolated room temperature resistivity ($\rho(298$ K)), slope of resistivity with temperature ($\frac{d\rho}{dT}$), and Debye Temperature (θ_D) as calculated with the Bloch-Gruneisen model, for a set of thin Au nanowires. Literature values for bulk gold are given in the last row.

W (nm)	$\rho(298$ K) ($\mu\Omega \cdot cm$)	$\frac{d\rho}{dT}$ ($\mu\Omega \cdot cm / K$)	θ_D (K)
24.0	42	0.0027	58.9
40.3	25	0.0024	64.7
52.6	21	0.0022	71.7
Bulk	2.4	0.0008	165

set of devices of varying length and fixed width ($W = 40$ nm). This data set enabled us to fit a value for our oxide substrate thermal conductivity, $\kappa_{ox}(T)$, at each temperature point. The fitting procedure takes as an input the average measured values of ρ and $d\rho/dT$ for this geometry. Some devices were discarded from the procedure due to anomalous slope or resistance values. The average measured self-heating slope versus wire length, with error bars representing standard error of the mean, and the prediction of the fitted model are shown in Fig. 5a for the set of temperature points in the experiment. Note that the vertical error bars do not represent the full uncertainty in the fitted data because they neglect error in ρ and $d\rho/dT$.

Figure 5b shows our fit $\kappa_{ox}(T)$ for 22 nm thick oxide (red data points) together with the result of previous work from Ref. 36. As compared to bulk oxide, thin oxide films can have significantly decreased effective thermal conductivities due to the higher defect density and potentially less ordered microstructure^{36,37}. Additionally, the contribution from thermal contact resistance on both sides of the thin oxide becomes significant relative

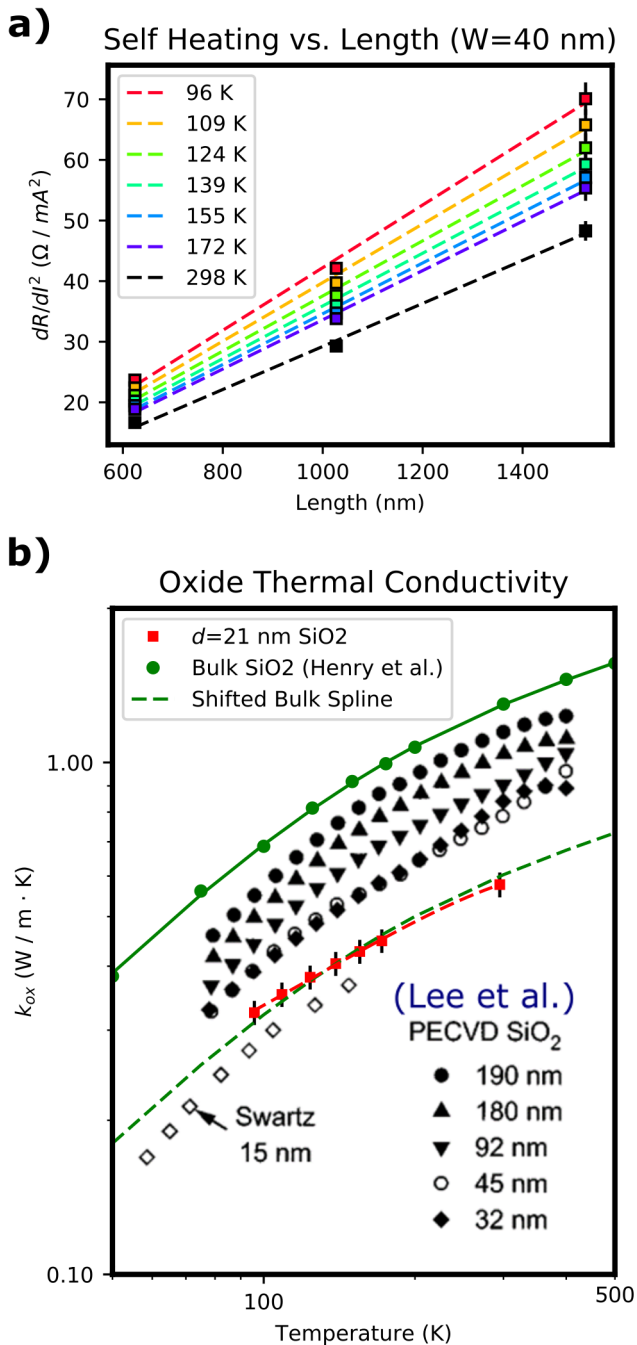


FIG. 5. Fitting the self-heating slope versus length (at fixed width) to extract κ_{ox} and κ_n at different temperatures (a) and our resulting estimate of $\kappa_{ox}(T)$ together with other thin-film silicon dioxide thermal conductivity estimates from Ref. 36 (b). Some components of the figure in (b) are reprinted with permission from the authors.

to the intrinsic thermal conductivity.

As noted by Lee et al.³⁶, for thin films the κ_{ox} versus temperature curves on log-log scale seem to have the same shape, but shifted downward by some fixed amount for each thickness. Indeed, we see that our fit oxide ther-

mal conductivity curve is very well described by the curve for bulk Au simply translated downward (dashed green line). For the following analyses we evaluate $\kappa_{ox}(T)$ between 95 and 300 K by a simple spline fit to our data (red dashed line).

C. Thermal Conductivity and Lorenz Number of Nanowires

For another set of wire widths, each with a fixed length, we made measurements of self-heating slope at temperatures ranging from 95 to 260 K. For each width we measured multiple devices in this fashion obtaining slope, ρ and $d\rho/dT$, then the estimate of κ_n versus temperature is taken as the average of the $\kappa_n(T)$ values computed for individual devices using splined $\kappa_{ox}(T)$ values. The model does not permit a closed-form expression for κ_n , so the values were obtained using a numerical solver for the transcendental relationship of Eq. (2).

The results of the thermal conductivity calculation are shown in Fig. 6a with error bars representing standard error of the mean. Compared to bulk gold, the nanowire thermal conductivity is more than an order of magnitude smaller and increases by almost 100% between 100 and 300 K, while k_{bulk} decreases very slightly with increasing temperature. Similar general behavior for thermal conductivity in this temperature range has been seen across several prior studies of nanowires^{8,10,22} and nanofilms^{21,38,39}.

In nanoscale metal systems structural scattering strongly degrades the electron thermal current and thus globally depresses κ_n at all temperatures relative to the bulk value. The temperature dependence of κ_n can be elucidated by considering the diffusive, free electron approximation¹³

$$\kappa_e = \frac{1}{3} c_e \nu_f \lambda = \frac{1}{3} \frac{m \nu_f^2 c_e}{n e^2 \rho},$$

$$\frac{d\kappa_e}{dT} \propto -c_e \frac{1}{\rho^2} \frac{d\rho}{dT} + \frac{1}{\rho} \frac{dc_e}{dT}, \quad (4)$$

where m is the electron mass, ν_f is the Fermi velocity, n is the free electron density, λ is the electron mean free path, and c_e is the electronic specific heat per unit volume. In this temperature regime c_e increases linearly¹³ and the two terms of Eq. (4) compete in determining the sign of the derivative. In the bulk system the fractional change in the resistivity, $\frac{d\rho}{dT}/\rho$, is large, and the first term dominates, yielding a *decreasing* thermal conductivity with temperature. Due to the vastly enhanced structural scattering in our nanowires, ρ is much larger and the fractional change in the resistivity and mean free path (MFP) is much smaller than in bulk, so that the first term is suppressed more strongly than the second term and the sign of $d\kappa_e/dT$ is reversed. Assuming that ν_f , n and c_e do not differ substantially between the bulk and

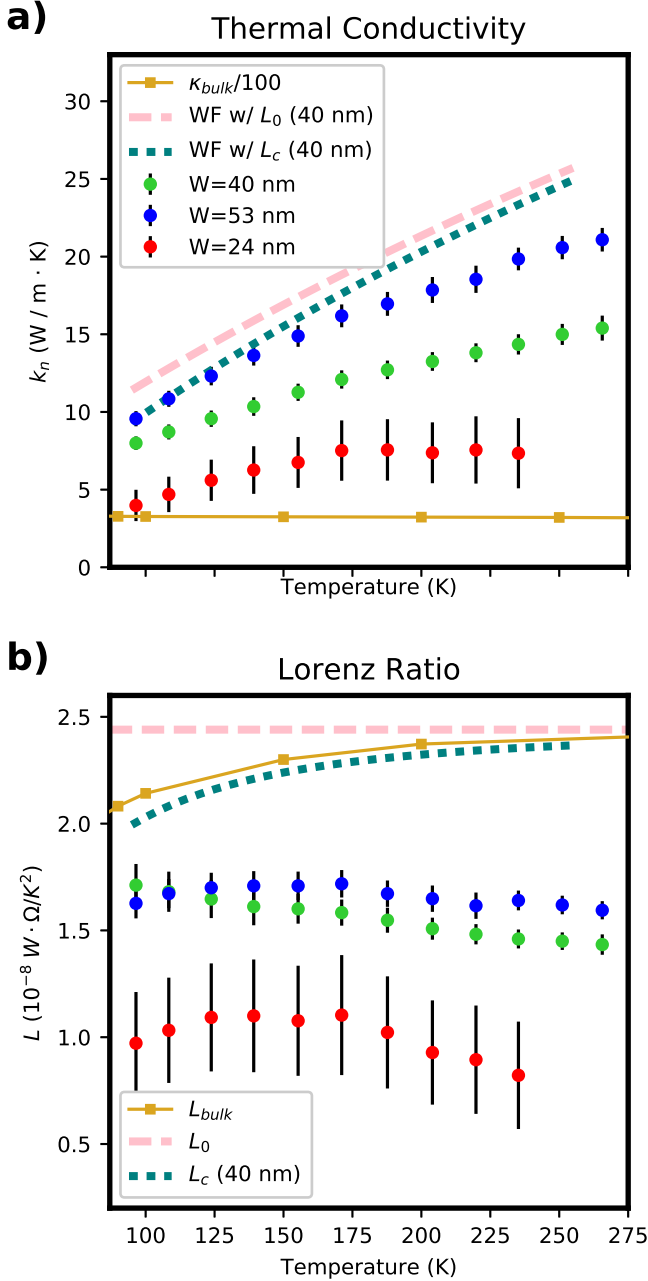


FIG. 6. Estimates of nanowire thermal conductivity (a) and calculated Lorenz ratio (b) versus temperature for several wire widths. Literature bulk gold values for the same are given by the solid gold lines (L_{bulk} from Ref. 40 and κ_{bulk} from Ref. 41). Also shown are Wiedemann-Franz predictions for our 40 nm wires using L_0 (dashed pink line) and L_c corrected for small-angle scattering (dotted teal line).

nanowire, and supplying values from Table I, we find for the weakest case ($W = 52$ nm) that the first term in Eq. (4) is only 4% of the bulk value while the second term is 11% of the bulk value.

This hypothesis is consistent with our observed trend of decreasing κ with decreasing width, and with our esti-

mation in Section III A that structural scattering appears dominant even up to 250 K. If we assume the WF Law holds, then for our wires in the regime of linear resistivity we expect $\kappa_e = L_0 \frac{T}{\frac{d\rho}{dT}T + \rho_0}$: this is plotted on Fig. 6a (dashed pink line) using our measured values for $d\rho/dT$ and ρ_0 for the 40 nm wires. We see the general shape is similar to our findings, but the values are significantly higher, implying the value of L_0 is too large to correctly describe our data within WF.

For all the nanowire widths the calculated Lorenz ratios $L = \rho\kappa/T$, shown in Fig. 6b, are relatively constant over temperature but are substantially depressed relative to bulk gold, particularly for the smallest width. A theoretical expression for a corrected Lorenz factor, L_c , which takes into account the effect of small-angle scattering within the Debye phonon model is given by^{14,16}

$$L_c = L_0 \left[1 + \frac{3}{\pi^2} \left(\frac{2}{Z} \right)^{2/3} \cdot \left(\frac{\theta_D}{T} \right)^2 \right]^{-1}, \quad (5)$$

where Z is the metal valence and θ_D is the Debye temperature. This correction should be increasingly unimportant as temperature increases relative to θ_D , due to heavily populating the higher energy phonon modes which give large-angle scattering. The T -dependent L_c and the corresponding predicted κ_n for our 40 nm wires are shown by the teal dotted lines in Fig. 6 (L_c computed with $Z = 1$ and the estimated θ_D for $W = 40$ nm).

Our inferred Lorenz ratios are still significantly lower than predicted by the small-angle correction, and furthermore they exhibit no strong T -dependence. This may suggest that in our system small angle inelastic scattering is significant relative to large angle scattering even up to 250 K, or some additional physical process suppresses electronic thermal current much more strongly than charge current.

We expect that the vibrational density of states for our structures is significantly distorted relative to bulk, and it may be the case that the population of small wave-vector phonons is disproportionately enhanced and small-angle scattering is much more prominent. In gold nanoparticles and nanocrystalline films, for instance, the presence of low-frequency, spatially confined, vibrations known as Lamb Modes have been theoretically predicted and experimentally observed⁴²⁻⁴⁴. Because we do not use an adhesion layer for our ultrathin gold on oxide the resulting deposited layer is highly granular, and we limit the temperature in all subsequent fabrication steps and chip handling to prevent any thermal annealing. It is possible that our ultrathin gold layer might support localized Lamb-like vibrations, which could participate in small-angle inelastic scattering with electrons while not contributing significantly to the phonon thermal current.

Finally, we illustrate how important it is to correctly incorporate substrate heat sinking in the thermal model by comparing the estimated curves for L derived by our full substrate-coupled model versus the model used in Refs. 8 and 9 for suspended wires. We also include a

comparison to a third estimation method which ignores the temperature dependence of κ_{ox} and uses just a single experimentally-determined value for room temperature, $\kappa_{ox}(T = 293 \text{ K})$. The results from applying the three different methods to the data for $W = 52 \text{ nm}$ wires are compared in Fig. 7. We note that in addition to being most physically correct, our method incorporating an approximation to $\kappa_{ox}(T)$ gives Lorenz number behavior most similar to other metallic systems: relatively constant over temperature and having a value nearest to bulk gold.

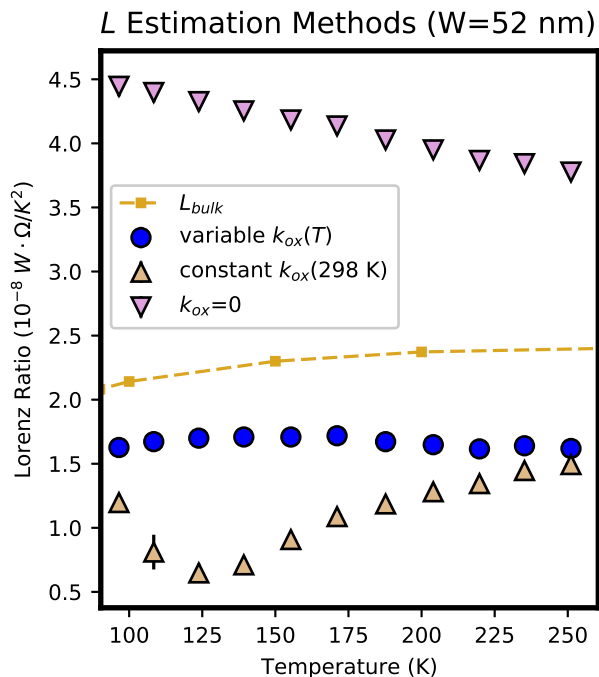


FIG. 7. Comparison of Lorenz ratio calculated under three different estimation methods: our full thermal model with substrate heat sinking (blue circles), assuming zero substrate heat sinking (violet downward triangles) and assuming a temperature-independent oxide thermal conductivity (beige triangles)

IV. CONCLUSION

Analysis of the temperature-dependent resistivity of our devices reveals the following picture of ultrathin, adhesion-layer-free, polycrystalline gold nanowires: The significantly increased granularity and surface area to volume ratio results in a strongly softened phonon dispersion as indicated by Debye temperatures as low as 35% of the bulk value. Despite the increased ease of thermal phonon occupancy, strong structural (grain boundary, surface and impurity) scattering still dominates the electron MFP even up to 250 K, contributing 75% of the total resistivity in the weakest case.

Consequent to this dominant structural scattering, the resistivity (and corresponding electron MFP) exhibits only a slight fractional change with temperature, which leads to a thermal conductivity whose temperature-dependence reflects primarily the linearly *increasing* electronic heat capacity. This is in sharp contrast to the crystalline bulk metal, where the heat capacity effect is outweighed by the fractional decrease in MFP due to enhanced electron-phonon scattering. However, within standard WF theory, the global decrease of MFP due to the structural scattering is not alone sufficient to explain how low the observed κ_n values are.

The failure of conventional WF to explain our suppressed κ_n is revealed by the anomalously low values computed for Lorenz ratio, which are much less than L_{bulk} and imply some physical process that relaxes the electronic thermal current much more effectively than the charge current. Small-angle scattering with low- q phonons has this effect in bulk metals at low temperatures, but incorporating this temperature-dependent scattering in the expression for L within the Debye phonon model cannot explain the full extent of the decrease in L for our wires. We posit that the highly granular, interface-dominated nature of our gold nanowires results in a vibrational density of states with greatly enhanced presence of localized, low- q modes, which are fully occupied over the temperature range of our experiments.

ACKNOWLEDGMENTS

This research was supported by the National Science Foundation [grant number 1309898]. We wish to acknowledge the help of M. Rooks at Yale YINQE and the Yale SEAS cleanroom staff in fabricating our devices. We also acknowledge substantial aid from Z. Kobos in maintaining the cryostat apparatus as well as many helpful discussions regarding electronics setup.

* sonya.sawtelle@yale.edu

¹ A. F. Mayadas and M. Shatzkes, “Electrical-resistivity model for polycrystalline films - case of arbitrary reflection

at external surfaces,” *Physical Review B* **1**, 1382 (1970).

² K. Fuchs, “The conductivity of thin metallic films according to the electron theory of metals,” *Proceedings of the*

- Cambridge Philosophical Society **34**, 100–108 (1938).
- ³ E. H. Sondheimer, “The mean free path of electrons in metals,” *Advances in Physics* **1**, 1–42 (1952).
 - ⁴ C. Durkan and M. E. Welland, “Size effects in the electrical resistivity of polycrystalline nanowires,” *Physical Review B* **61**, 14215–14218 (2000).
 - ⁵ Daniel Josell, Sywert H. Brongersma, and Zsolt Tokei, “Size-dependent resistivity in nanoscale interconnects,” *Annual Review of Materials Research* **39**, 231–254 (2009).
 - ⁶ J. S. Chawla, F. Gstrein, K. P. O’Brien, J. S. Clarke, and D. Gall, “Electron scattering at surfaces and grain boundaries in Cu thin films and wires,” *Physical Review B* **84**, 235423 (2011).
 - ⁷ A. Bid, A. Bora, and A. K. Raychaudhuri, “Temperature dependence of the resistance of metallic nanowires of diameter $\zeta = 15$ nm: Applicability of Bloch-Grüneisen theorem,” *Physical Review B* **74**, 035426 (2006).
 - ⁸ Z. Cheng, L. J. Liu, S. Xu, M. Lu, and X. W. Wang, “Temperature dependence of electrical and thermal conduction in single silver nanowire,” *Scientific Reports* **5**, 10718 (2015).
 - ⁹ F. Volklein, H. Reith, T. W. Cornelius, M. Rauber, and R. Neumann, “The experimental investigation of thermal conductivity and the Wiedemann-Franz law for single metallic nanowires,” *Nanotechnology* **20**, 325706 (2009).
 - ¹⁰ M. N. Ou, T. J. Yang, S. R. Harutyunyan, Y. Y. Chen, C. D. Chen, and S. J. Lai, “Electrical and thermal transport in single nickel nanowire,” *Applied Physics Letters* **92**, 063101 (2008).
 - ¹¹ D. Kojda, R. Mitdank, M. Handweg, A. Mogilatenko, M. Albrecht, Z. Wang, J. Ruhhammer, M. Kroener, P. Woias, and S. F. Fischer, “Temperature-dependent thermoelectric properties of individual silver nanowires,” *Physical Review B* **91**, 024302 (2015).
 - ¹² J. L. Wang, Z. H. Wu, C. K. Mao, Y. F. Zhao, J. K. Yang, and Y. F. Chen, “Effect of electrical contact resistance on measurement of thermal conductivity and Wiedemann-Franz law for individual metallic nanowires,” *Scientific Reports* **8**, 4862 (2018).
 - ¹³ Neil W. Ashcroft and N. David Mermin, *Solid State Physics*, 1st ed. (Brooks/Cole, 1976).
 - ¹⁴ N. Stojanovic, D. H. S. Maithripala, J. M. Berg, and M. Holtz, “Thermal conductivity in metallic nanostructures at high temperature: Electrons, phonons, and the Wiedemann-Franz law,” *Physical Review B* **82**, 075418 (2010).
 - ¹⁵ R. E. B. Makinson, “The thermal conductivity of metals,” *Proceedings of the Cambridge Philosophical Society* **34**, 474–497 (1938).
 - ¹⁶ P. G. Klemens and R. K. Williams, “Thermal conductivity of metals and alloys,” *International Metals Reviews* **31**, 197–215 (1986).
 - ¹⁷ Y. Zhang, N. P. Ong, Z. A. Xu, K. Krishana, R. Gagnon, and L. Taillefer, “Determining the Wiedemann-Franz ratio from the thermal Hall conductivity: Application to Cu and YBa₂Cu₃O_{6.95},” *Physical Review Letters* **84**, 2219–2222 (2000).
 - ¹⁸ A. Principi and G. Vignale, “Violation of the Wiedemann-Franz law in hydrodynamic electron liquids,” *Physical Review Letters* **115**, 056603 (2015).
 - ¹⁹ J. M. Ziman, “Electronic conduction in metals,” in *Electrons and Phonons: The Theory of Transport Phenomena in Solids* (Oxford University Press, Oxford, 2001) Book section Electronic Conduction in Metals.
 - ²⁰ S. Lee, K. Hippalgaonkar, F. Yang, J. W. Hong, C. Ko, J. Suh, K. Liu, K. Wang, J. J. Urban, X. Zhang, C. Dames, S. A. Hartnoll, O. Delaire, and J. Q. Wu, “Anomalously low electronic thermal conductivity in metallic vanadium dioxide,” *Science* **355**, 371– (2017).
 - ²¹ Q. G. Zhang, B. Y. Cao, X. Zhang, M. Fujii, and K. Takahashi, “Influence of grain boundary scattering on the electrical and thermal conductivities of polycrystalline gold nanofilms,” *Physical Review B* **74**, 134109 (2006).
 - ²² S. Yoneoka, J. Lee, M. Liger, G. Yama, T. Kodama, M. Gunji, J. Provine, R. T. Howe, K. E. Goodson, and T. W. Kenny, “Electrical and thermal conduction in atomic layer deposition nanobridges down to 7 nm thickness,” *Nano Letters* **12**, 683–686 (2012).
 - ²³ Z. Li, Q. Sun, X. D. Yao, Z. H. Zhu, and G. Q. Lu, “Semiconductor nanowires for thermoelectrics,” *Journal of Materials Chemistry* **22**, 22821–22831 (2012).
 - ²⁴ A. I. Hochbaum, R. K. Chen, R. D. Delgado, W. J. Liang, E. C. Garnett, M. Najarian, A. Majumdar, and P. D. Yang, “Enhanced thermoelectric performance of rough silicon nanowires,” *Nature* **451**, 163–U5 (2008).
 - ²⁵ E. Z. Xu, Z. Li, J. A. Martinez, N. Sinitsyn, H. Htoon, N. Li, B. Swartzentruber, J. A. Hollingsworth, J. Wang, and S. X. Zhang, “Diameter dependent thermoelectric properties of individual single nanowires,” *Nanoscale* **7**, 2869–2876 (2015).
 - ²⁶ J. Zou and A. Balandin, “Phonon heat conduction in a semiconductor nanowire,” *Journal of Applied Physics* **89**, 2932–2938 (2001).
 - ²⁷ S. Karg, P. Mensch, B. Gotsmann, H. Schmid, P. Das Kanungo, H. Ghoneim, V. Schmidt, M. T. Bjork, V. Troncale, and H. Riel, “Measurement of thermoelectric properties of single semiconductor nanowires,” *Journal of Electronic Materials* **42**, 2409–2414 (2013).
 - ²⁸ D. Patrick Hunley, Stephen L. Johnson, Roel L. Flores, Abhishek Sundararajan, and Douglas R. Strachan, “Analytical model for self-heating in nanowire geometries,” *Journal of Applied Physics* **113**, 234306 (2013).
 - ²⁹ C. Durkan, M. A. Schneider, and M. E. Welland, “Analysis of failure mechanisms in electrically stressed Au nanowires,” *Journal of Applied Physics* **86**, 1280–1286 (1999).
 - ³⁰ Francois Leonard, “Reduced joule heating in nanowires,” *Applied Physics Letters* **98**, 103101 (2011).
 - ³¹ T. Westover, R. Jones, J. Y. Huang, G. Wang, E. Lai, and A. A. Talin, “Photoluminescence, thermal transport, and breakdown in joule-heated GaN nanowires,” *Nano Letters* **9**, 257–263 (2009).
 - ³² G. Kastle, H. G. Boyen, A. Schroder, A. Plettl, and P. Ziemann, “Size effect of the resistivity of thin epitaxial gold films,” *Physical Review B* **70**, 165414 (2004).
 - ³³ G. D. Marzi, D. Iacopino, A. J. Quinn, and G. Redmond, “Probing intrinsic transport properties of single metal nanowires: Direct-write contact formation using a focused ion beam,” *Journal of Applied Physics* **96**, 3458–3462 (2004).
 - ³⁴ M. X. Gu, C. Q. Sun, Z. Chen, T. C. Au Yeung, S. Li, C. M. Tan, and V. Nosik, “Size, temperature, and bond nature dependence of elasticity and its derivatives on extensibility, Debye temperature, and heat capacity of nanostructures,” *Physical Review B* **75**, 125403 (2007).
 - ³⁵ W. G. Ma, X. Zhang, and K. Takahashi, “Electrical properties and reduced Debye temperature of polycrystalline thin gold films,” *Journal of Physics D-Applied Physics* **43**,

- 134109 (2010).
- ³⁶ S. M. Lee and D. G. Cahill, “Heat transport in thin dielectric films,” *Journal of Applied Physics* **81**, 2590–2595 (1997).
- ³⁷ M. B. Kleiner, S. A. Kuhn, and W. Weber, “Thermal conductivity measurements of thin silicon dioxide films in integrated circuits,” *Ieee Transactions on Electron Devices* **43**, 1602–1609 (1996).
- ³⁸ H. D. Wang, J. H. Liu, X. Zhang, and K. Takahashi, “Breakdown of wiedemann-franz law in individual suspended polycrystalline gold nanofilms down to 3 k,” *International Journal of Heat and Mass Transfer* **66**, 585–591 (2013).
- ³⁹ X. Zhang, H. Q. Xie, M. Fujii, H. Ago, K. Takahashi, T. Ikuta, H. Abe, and T. Shimizu, “Thermal and electrical conductivity of a suspended platinum nanofilm,” *Applied Physics Letters* **86**, 171912 (2005).
- ⁴⁰ J.G. Hust Sparks and L.L., *Lorenz Ratios of Technically Important Metals and Alloys*, Report (National Bureau of Standards, 1973).
- ⁴¹ C.Y. Ho R.W. Powell and P.E. Liley, *Thermal Conductivity of Selected Materials*, Report (National Bureau of Standards, 1966).
- ⁴² R. Carles, P. Benzo, B. Pecassou, and C. Bonafos, “Vibrational density of states and thermodynamics at the nanoscale: the 3d-2d transition in gold nanostructures,” *Scientific Reports* **6**, 39164 (2016).
- ⁴³ A. Crut, P. Maioli, N. Del Fatti, and F. Vallee, “Acoustic vibrations of metal nano-objects: Time-domain investigations,” *Physics Reports-Review Section of Physics Letters* **549**, 1–43 (2015).
- ⁴⁴ P. M. Derlet, R. Meyer, L. J. Lewis, U. Stuhr, and H. Van Swygenhoven, “Low-frequency vibrational properties of nanocrystalline materials,” *Physical Review Letters* **87**, 205501 (2001).